

Magnonic Analogs of Topological Dirac Semimetals

S. A. Owerre¹

¹*Perimeter Institute for Theoretical Physics, 31 Caroline St. N., Waterloo, Ontario N2L 2Y5, Canada.**

(Dated: November 24, 2023)

In electronic topological Dirac semimetals the conduction and valence bands touch at discrete points in the Brillouin zone and form Dirac cones. They are robust against spin-orbit interaction (SOI) and protected by crystal symmetries. They can be driven to different topological phases by breaking the symmetries. In the low-temperature quantum magnetic systems the magnon dispersions have similar band structures as the electron dispersions, but with positive definite energies. In these magnetic systems SOI manifests in the form of the Dzyaloshinskii-Moriya interaction (DMI). In this Communication, we identify two types of *magnonic Dirac semimetals* in quasi-two-dimensional quantum magnets. The first type is a consequence of topological phase transition between trivial and topological magnon insulators and the second type is intrinsic and protected by crystal symmetries. They are robust against DMI and can be driven to a topological magnon phase by breaking the symmetries. They can be manipulated by an external magnetic field and accessible by the bulk sensitive inelastic neutron scattering experiments.

I. INTRODUCTION

Topological band theory in electronic systems has been the most dominant field in different branches of physics over the past decade [1–4]. The concept of topological band theory is realized in insulating electronic systems with a nontrivial gap in the energy band structures. A common feature of topological systems is the existence of gapless edge modes protected by a topological invariant quantity such as the Chern number and \mathbb{Z}_2 index [2]. This quantity distinguishes a nontrivial topological system from a trivial one. However, the transition between the two regimes requires a tunable gap closing point [5, 6]. The topological critical point realizes a massless Dirac Hamiltonian termed electronic Dirac semimetal (DSM). In recent studies it has been shown that electronic DSMs can manifest intrinsically in two-dimensional (2D) [7] and three-dimensional (3D) [8–10] SOI electronic systems. They are protected by time-reversal (\mathcal{T}) symmetry [7, 8] at the high symmetry points of the BZ and additional crystal symmetries [9, 10] when they occur away from the high symmetry points in the Brillouin zone (BZ). By breaking of symmetries it is possible to access other nontrivial topological electronic systems [11–14].

A rapidly developing field is the extension of topological concepts to nonelectronic bosonic systems such as magnons [15–30] and phonons [31–39]. Unlike electronic systems these bosonic quasi-particles are charge-neutral which makes them potential candidates to design systems with low-dissipation and good coherent transport applicable to spin-based computing and magnon spintronics [40]. They also do not have conduction and valence bands because the negative energy solution has no physical meaning. Therefore linear band crossing points must occur at finite energy. For magnons which are spin-1 bosonic excitations of ordered quantum mag-

nets, the DMI [41, 42] induces topological magnon bands [22, 23, 26–29] in the same way that SOI induces topological bands in electronic systems [1–4]. The DMI stems from SOI [42] and it is present in magnetic materials that lack an inversion center. The kagomé lattice is built with this structure, because the midpoint of the bonds connecting two nearest-neighbour magnetic ions is not a center of inversion. This leads to topological magnon effects in ferromagnetic kagomé lattice [22, 23]. A broken inversion center is also present on the honeycomb lattice between the midpoints of second nearest-neighbour magnetic ions. Therefore a DMI is allowed on the second nearest-neighbour bonds of the honeycomb lattice, and topological magnon effects are manifested as recently proposed [27, 28]. In insulating ferromagnets the DMI is the primary source of magnon thermal Hall effect which has been observed experimentally in different ferromagnets [15–17] and the first topological magnon bands has been observed in quasi-2D kagomé ferromagnet Cu(1,3-bdc) [18]. In recent studies, however, the concept of Weyl magnons (WMs) have been proposed in magnetically ordered systems in 3D pyrochlore ferromagnets [43–45] and antiferromagnets [46]. Therefore there is a possibility of *magnonic DSMs* in magnetic systems with DMI.

We note that WMs in 3D pyrochlore ferromagnets with DMI [43, 44] breaks \mathcal{T} -symmetry macroscopically and possess magnon thermal Hall effect [15, 16]. In contrast, the *magnonic DSMs* with DMI preserve a combination of certain symmetries which prohibit a finite magnon thermal Hall effect. As we do not expect every ordered insulating quantum magnetic system with DMI to possess a finite thermal magnon Hall effect, it is reasonable that the concept of *magnonic DSMs* should exist. Just like in electronic systems they exist in two forms. The first one is a consequence of topological phase transition between trivial and topological insulators [5], and the second one is intrinsic due to additional symmetries such as rotational, translational, and mirror symmetries [9, 10]. The first type is manifested in quasi-2D systems such as the collinear

*Electronic address: sowerre@perimeterinstitute.ca

honeycomb and kagomé ferromagnets, as well as field-induced canted/non-collinear magnetic order in honeycomb (anti)ferromagnets. The second type is manifested in the coplanar/non-collinear $\mathbf{Q} = \mathbf{0}$ long-range magnetic order in frustrated magnets such as the kagomé and star antiferromagnets. They exhibit nearly flat chiral magnon edge modes which connect the bulk Dirac magnon cones and they can be driven to a topological magnon phase with finite thermal Hall conductivity by breaking of symmetries. We propose different relevant quasi-2D experimental materials such as single crystals of honeycomb magnets $\text{Bi}_3\text{Mn}_4\text{O}_{12}(\text{NO}_3)$ [47], CaMn_2Sb_2 [48], APS_3 ($A=\text{Mn, Fe}$) [49–52], CrBr_3 [53, 54], $\text{BaM}_2((\text{XO})_4)_2$ ($M=\text{Co, Ni}$; $X=\text{P, As}$) [55, 56], etc., kagomé ferromagnet $\alpha\text{-MgCu}_3(\text{OD})_6\text{Cl}_2$ [57], kagomé jarosite antiferromagnets [58–61] such as $\text{KCr}_3(\text{OH})_6(\text{SO}_4)_2$ [61, 62] and $\text{KFe}_3(\text{OH})_6(\text{SO}_4)_2$ [63, 64], etc., and star-lattice magnets [65]. This work will rekindle the re-examination of magnetic excitations in quantum magnetic systems both theoretically and experimentally.

II. DISTORTED FERROMAGNETS

A. Model

The most common bipartite quantum magnet is the honeycomb lattice. We first consider collinear ferromagnetic order on this lattice. The Hamiltonian can be written as

$$\mathcal{H} = - \sum_{ij} J_{ij} \mathbf{S}_i \cdot \mathbf{S}_j + \sum_{\langle\langle ij \rangle\rangle} \mathbf{D}_{ij} \cdot \mathbf{S}_i \times \mathbf{S}_j, \quad (1)$$

where \mathbf{S}_i are the spin moments, $J_{ij} > 0$ are ferromagnetic distorted interactions with $J_{ij} = J_1, J_2, J_3$ along $\delta_1, \delta_2, \delta_3$ respectively. Here, $J_{ij} = J'$ along δ' as depicted in Fig. 1 connecting the third-nearest neighbours. The second term is a uniform out-of-plane staggered DMI between sites i and j , with $\mathbf{D}_{ij} = \nu_{ij} D \hat{\mathbf{z}}$ and $\nu_{ij} = -\nu_{ji} = \pm 1$. The DMI is allowed because of the inversion symmetry breaking between the bonds of the second-nearest neighbours on the honeycomb lattice. It should be noted that the ground state of Eq. 1 remains a ferromagnetic insulator despite the presence of the DMI. The isotropic point $J_{ij} = J$, $J' = 0$ has been previously studied in the context of topological magnon insulator [27] and the associated thermal Hall effect [28] and spin Nernst effect [29]. In this limit the *magnonic DSMs* and the topological magnon phase transition we propose here are not possible.

In this paper we will be interested in the ordered phases of quantum magnets at low-temperatures in which the term magnon can be used. In this regime, the standard noninteracting Holstein-Primakoff (HP) spin-boson

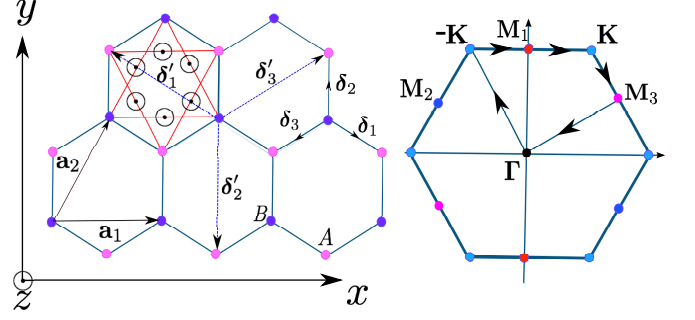


FIG. 1: Color online. (Left) The geometry of honeycomb lattice. The nearest-neighbour vectors are $\delta_1 = a \left(\frac{\sqrt{3}}{2}, -\frac{1}{2} \right)$, $\delta_2 = a (0, 1)$, $\delta_3 = -a \left(\frac{\sqrt{3}}{2}, \frac{1}{2} \right)$. The DMI is allowed at the midpoints of the second-nearest neighbours indicated by circle dots which leads to fictitious magnetic flux in momentum space. The blue dash lines connect the third nearest neighbours with $\delta'_1 = a (-\sqrt{3}, 1)$, $\delta'_2 = a (0, -2)$, $\delta'_3 = a (\sqrt{3}, 1)$. (Right) The Brillouin zone of the honeycomb lattice. Points with the same color are related by symmetry.

transformation is valid:

$$S_{i,\alpha}^z = S - b_{i,\alpha}^\dagger b_{i,\alpha}, \quad (2)$$

$$S_{i,\alpha}^y = i \sqrt{\frac{S}{2}} (b_{i,\alpha}^\dagger - b_{i,\alpha}), \quad (3)$$

$$S_{i,\alpha}^x = \sqrt{\frac{S}{2}} (b_{i,\alpha}^\dagger + b_{i,\alpha}), \quad (4)$$

where $b_{i,\alpha}^\dagger (b_{i,\alpha})$ are the bosonic creation (annihilation) operators and $\alpha = A, B$ label the two sublattices on the honeycomb lattice denoted by different colors in Fig. 1. The Hamiltonian in momentum space can be represented by $\mathcal{H} = \sum_{\mathbf{k}} \Psi_{\mathbf{k}}^\dagger \mathcal{H}(\mathbf{k}) \Psi_{\mathbf{k}} + \text{const.}$, where $\Psi_{\mathbf{k}} = (b_{A\mathbf{k}}^\dagger, b_{B\mathbf{k}}^\dagger)$ and

$$\mathcal{H}(\mathbf{k}) = v_0 \mathbb{I}_{2 \times 2} + S \sum_{a=1}^3 d_a(\mathbf{k}) \sigma_a, \quad (5)$$

where $\mathbb{I}_{2 \times 2}$ is an identity 2×2 matrix,

$$d_1(\mathbf{k}) = -4J \cos \tilde{k}_x \cos \tilde{k}_y - 2(J_2 + 2J' \cos \sqrt{3} \tilde{k}_x) \cos k_y \quad (6)$$

$$- 2J' \cos 2k_y,$$

$$d_2(\mathbf{k}) = -2(J_2 + 2J' \cos \sqrt{3} \tilde{k}_x - 2J' \cos k_y) \sin k_y \quad (7)$$

$$+ 4J \cos \tilde{k}_x \sin \tilde{k}_y,$$

$$d_3(\mathbf{k}) = 4D(\cos \tilde{k}_x - \cos 3\tilde{k}_y) \sin \tilde{k}_x, \quad (8)$$

where $v_0 = SJ_{ij}$, σ_a are the sublattice pseudo-spin Pauli matrices, $\tilde{k}_x = \sqrt{3}k_x/2$ and $\tilde{k}_y = k_y/2$. We have used $J_1 = J_3 = J$ and $S = 1/2$. This model can be regarded as the magnonic analog of Haldane insulator [1], but the present model is not restricted to graphene-like materials since all the interactions might be present in quantum magnetic materials.

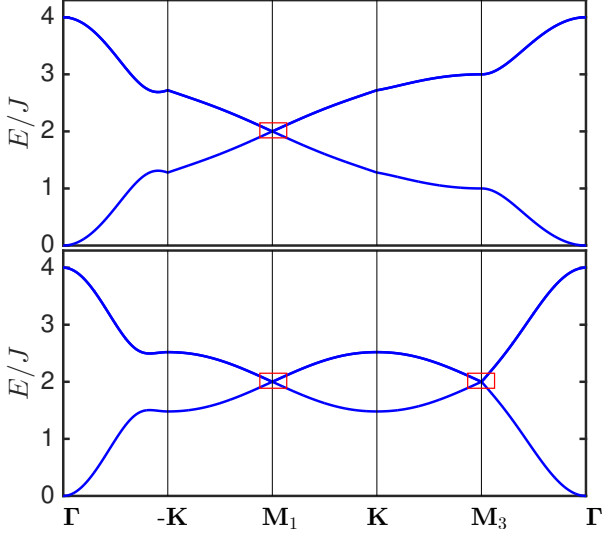


FIG. 2: Color online. Magnon band dispersions of distorted honeycomb ferromagnets for $D/J = 0.2$ and two values of lattice distortion. (Top) $J'/J = 0$, $J_2 = J_2^c$. (Bottom) $J' = J_2^c$, $J_2 = J$. The rectangles indicate Dirac nodes at the high symmetry points of the Brillouin zone.

B. Tunable magnonic Dirac semimetal

In this section, we present the first type of *magnonic DSMs*, which results from a topological phase transition between trivial and topological magnon insulators. We commence with the case of zero DMI, $D = 0$ and $J' = 0$. The isotropic limit ($J_2 = J$, $J' = 0$) exhibits gapless nodes at two inequivalent Dirac points $\pm\mathbf{K}$ [66]. In the distorted case ($J_2 \neq J$, $J' = 0$) the two inequivalent Dirac points remain stable but move away from the $\pm\mathbf{K}$ points for $J < J_2 < 2J$. They subsequently annihilate each other at $J_2 = J_2^c = 2J$ and emerge as a single Dirac point at \mathbf{M}_1 . A gap opens for $J_2 > J_2^c$ and the system becomes a trivial insulator with a gap of $\Delta_{\mathbf{M}_1} = 2|J_2 - J_2^c|$ and $\Delta_{\mathbf{K}} = 2|J_2 - J|$ at \mathbf{M}_1 and \mathbf{K} respectively. It should be noted that lattice distortion preserves both \mathcal{T} and inversion (\mathcal{I}) symmetries. This is similar to graphene [67, 68]. Nevertheless, the present model is a quantum magnetic system which can be realized in different materials. The shifted Dirac points for $J_2 < J_2^c$ are located at $\mathbf{G}_0 = (\pm k_x^0, 0)$, where $\cos(\sqrt{3}k_x^0/2) = -J_2/J_2^c$.

The main purpose of this study is the possibility of Dirac points that cannot be gapped by the DMI or SOI [7]. As noted above, this is not possible at the isotropic limit [27–29]. Let us consider the effects of nonzero DMI at $J' = 0$. We note that the spontaneous magnetization of ferromagnetic order has already broken \mathcal{T} -symmetry. However, the DMI also breaks the \mathcal{T} -symmetry of $\mathcal{H}(\mathbf{k})$ explicitly and macroscopically, hence it is expected to gap the Dirac magnon points and drives the system into a topological phase [27–29]. These two types of \mathcal{T} -symmetry breaking differ mathematically in momentum

space. In the former $\mathcal{H}(\mathbf{k})$ does not break \mathcal{T} -symmetry even though the ferromagnetic order has already broken \mathcal{T} -symmetry. On the other hand, one finds that in the latter \mathcal{T} -symmetry of $\mathcal{H}(\mathbf{k})$ defined as $\Theta = i\sigma_y\mathcal{K}$ is broken explicitly and macroscopically where \mathcal{K} is complex conjugation. The top figure in Fig. 2 shows the magnon bands at nonzero DMI for two values of J_2 . A nonzero DMI breaks the degeneracy of the magnon bands everywhere except at \mathbf{M}_1 for $J_2 = J_2^c$. This critical point realizes a tunable *magnonic DSM*.

Expanding the momentum space Hamiltonian (5) around $\mathbf{k} = \mathbf{M}_1$ yields

$$\mathcal{H}(\mathbf{M}_1 + \mathbf{q}) = v_0\mathbb{I}_{2\times 2} + S\tilde{v}_a(\sigma_x - \tau\sqrt{3}\sigma_y) + S[\tilde{v}_z\sigma_zq_x + (\tau\tilde{v}_x\sigma_x + \tilde{v}_y\sigma_y)q_y], \quad (9)$$

where $\tau = \pm$ at $\pm\mathbf{M}_1$,

$$\tilde{v}_a = -2J + J_2, \quad \tilde{v}_x = \sqrt{3}(J + J_2), \quad (10)$$

$$\tilde{v}_y = J + J_2, \quad \tilde{v}_z = 4\sqrt{3}D. \quad (11)$$

We see that the gap at \mathbf{M}_1 is generated by a DMI independent term \tilde{v}_a . This is of interest because the DMI is an intrinsic anisotropy and not a tunable parameter, but lattice distortion can be tuned by applying a uniaxial strain [69, 70], for instance along the y - or δ_2 -direction. Besides, some materials may belong to the critical point $J_2 = J_2^c$ where the gap closes and the system is \mathcal{T} -invariant.

In real materials there is a possibility of additional interactions, which may also be distorted. However, since the Dirac magnon points in this case simply involves a tunable quantity, it suffices to consider a tunable undistorted additional interaction. We consider the effects of adding a symmetric isotropic third-nearest-neighbour interaction J' . We note that a symmetric isotropic second-nearest-neighbour interaction and Ising anisotropies may be present in real materials, however they merely rescale v_0 and lead to tilted Dirac magnon cones. The inclusion of J' introduces complexities in this model. The interesting case is the persistence of Dirac points in the presence of DMI or SOI [7]. The Dirac points at $\pm\mathbf{K}$ are gapped by the DMI, but the Dirac points at \mathbf{M}_1 are protected for $J' = J'_{1c} = (2J - J_2)/3$ and those at $\mathbf{M}_{2,3}$ are protected for $J' = J'_{2c} = J_2/3$. A clear picture of these points can be understood in the low-energy Hamiltonian. At \mathbf{M}_1 , only \tilde{v}_a in Eq. 9 is rescaled by $3J'$, and we recover a *magnonic DSM* at $J' = J'_{1c}$. Expanding around $\mathbf{k} = \mathbf{M}_{2,3}$ yields

$$\mathcal{H}(\mathbf{M}_{2,3} + \mathbf{q}) = v_0\mathbb{I}_{2\times 2} + S\tilde{v}'_a(\sigma_x + \sqrt{3}\sigma_y) + S[(\tilde{v}'_{xz}\sigma_z + v'_{xx}\sigma_x + \tau v'_{xy}\sigma_y)q_x + (\tau\tilde{v}'_{yz}\sigma_z + \tau v'_{yx}\sigma_x + v'_{yy}\sigma_y)q_y], \quad (12)$$

where $\tau = \pm$ at $\mathbf{M}_{2,3}$, $\tilde{v}'_a = 3J' - J_2$,

$$\tilde{v}'_{xx} = 3J, \quad \tilde{v}'_{xy} = -\sqrt{3}J_2, \quad \tilde{v}'_{xz} = -2\sqrt{3}D, \quad (13)$$

$$\tilde{v}'_{yx} = \sqrt{3}J_2, \quad \tilde{v}'_{yy} = -J_2, \quad \tilde{v}'_{yz} = 6D, \quad (14)$$

The gap \tilde{v}'_a closes at $J' = J'_{2c}$ yielding a *magnonic DSM* as shown in the bottom figure of Fig. 2.

For the kagomé ferromagnets a *magnonic DSM* can be achieved by a second-nearest-neighbour interaction or lattice distortion. Indeed, magnon-magnon interactions do not introduce additional terms that would break \mathcal{T} -symmetry, therefore the Dirac magnon points should be robust against higher order magnon interactions. The Dirac magnon points are protected by the critical values and \mathcal{T} -symmetry, which suggests that away from the critical values the system is likely to break \mathcal{T} -symmetry and transits to different magnon phases. These systems are examples of tunable *magnonic DSMs* at the phase transition point [5]. In the subsequent sections we will show that *magnonic DSMs* can also occur without tunable interactions or lattice distortion.

III. CANTED ANTIFERROMAGNETS

A. Model

In this section, we consider the possibility of linear band crossing in the field-induced canted Néel order on the honeycomb lattice governed by the Hamiltonian

$$\mathcal{H} = J \sum_{\langle ij \rangle} \mathbf{S}_i \cdot \mathbf{S}_j + \sum_{\langle\langle ij \rangle\rangle} \mathbf{D}_{ij} \cdot \mathbf{S}_i \times \mathbf{S}_j - H \sum_i S_i^z, \quad (15)$$

where J is an antiferromagnetic coupling. We have restricted the analysis to isotropic nearest-neighbour interaction only as it captures all the physics to be described. In other words, no tunable Heisenberg interactions will be considered. The last term is an external out-of-plane magnetic field along the z -axis. At zero magnetic field $H = 0$, the ground state of Eq. 15 is a collinear Néel order with the spins aligned antiparallel along the in-plane direction chosen as the x -axis. Although \mathcal{T} -symmetry is already broken by the Néel order, the coexistence of lattice translation \mathbf{T}_a and \mathcal{T} -symmetry leaves the collinear Néel order invariant. This leads to an analog of Kramers theorem [71] and the resulting magnon dispersions are doubly degenerate between the in-plane $\hat{\mathbf{x}}$ -antipolarized states $S_x = \pm S$. The out-of-plane DMI preserves this combined symmetry and does not lift the spin and magnon band degeneracy. Therefore the possibility of linear band crossing is not possible for a single degenerate magnon band. Nevertheless, the $U(1)$ symmetry of the Hamiltonian gives rise to spontaneous symmetry breaking with a linear Goldstone mode at the Γ -point, but this is not a linear band crossing and cannot be attributed to a Dirac magnon point with opposite winding number.

In the presence of an external magnetic field, the system first start from the collinear Néel order in the x - y plane and cant slightly along the magnetic field direction for $H < H_s$ as shown in Fig. 3 (right), where $H_s = 6JS$ is the saturation field. Unlike in collinear ferromagnets, there are two field-induced spin components — one parallel to the field $\mathbf{M} \parallel \mathbf{H}$ and the other perpendicular to

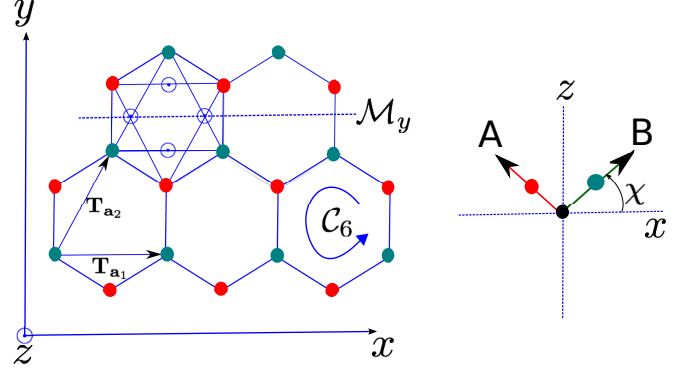


FIG. 3: Color online. (Left). The honeycomb lattice and the associated symmetries. (Right) Non-collinear (canted) Néel order induced by the magnetic field $\sin \chi \propto H$.

the field $\mathbf{M}_{st} \perp \mathbf{H}$, where \mathbf{M} and \mathbf{M}_{st} are the uniform and staggered magnetizations respectively (see Fig. 3). Therefore, we expect different magnon dispersions for each spin component. The former breaks $\mathcal{T}\mathbf{T}_a$ symmetry and the degeneracy of the magnon dispersions will be lifted. The latter preserves a combination of $\mathcal{T}\mathbf{T}_a$ and a π -rotation \mathcal{R}_π around the perpendicular-to-field spin-projections. In addition, the honeycomb lattice also has mirror symmetry \mathcal{M}_y and six-fold rotation symmetry \mathcal{C}_6 about the center of the hexagons as shown in Fig. 3. For the perpendicular-to-field spin-projections, we will show that there exist Dirac magnon nodes which are not lifted by the DMI, hence can be regarded as the *magnonic DSM*. This result will also manifest in other non-collinear bipartite structures since a canted/non-collinear magnetic order can also occur in easy-axis (anti)ferromagnets in a transverse in-plane magnetic field and also in easy-plane (anti)ferromagnets in a longitudinal out-of-plane magnetic field.

B. Field-induced magnonic Dirac semimetal

A tunable *magnonic DSM* can be induced by an external applied magnetic field instead of lattice distortion and exchange interactions. In fact, an applied magnetic field is more feasible experimentally. We proceed from Eq. 15 by rotating the coordinate axes by the canting angle χ about the y -axis such that the z -axis coincides with the local direction of the classical polarization [72]:

$$S_{i,A(B)}^x = \pm S_{i,A(B)}^{'x} \sin \chi \pm S_{i,A(B)}^{'z} \cos \chi, \quad (16)$$

$$S_{i,A(B)}^y = \pm S_{i,A(B)}^{'y}, \quad (17)$$

$$S_{i,A(B)}^z = -S_{i,A(B)}^{'x} \cos \chi + S_{i,A(B)}^{'z} \sin \chi, \quad (18)$$

where the primes denote the rotated coordinate and \pm applies to sublattices A and B respectively. The DMI can be resolved in two components due to magnetic-field-induced canting, that is $\mathbf{M} \parallel \mathbf{D} \parallel \mathbf{H}$ and $\mathbf{M}_{st} \parallel \mathbf{D} \perp \mathbf{H}$.

To linear order in spin wave theory, the two components are rescaled as

$$\mathcal{H}_{DMI}^{\parallel} = D^{\parallel} \sum_{\langle\langle ij \rangle\rangle} \nu_{ij} \hat{\mathbf{z}} \cdot \mathbf{S}'_i \times \mathbf{S}'_j, \quad (19)$$

$$\mathcal{H}_{DMI}^{\perp} = D^{\perp} \sum_{\langle\langle ij \rangle\rangle} \hat{\mathbf{z}} \cdot \mathbf{S}'_i \times \mathbf{S}'_j, \quad (20)$$

where $D^{\parallel} \rightarrow D \sin \chi$, $D^{\perp} \rightarrow D \cos \chi$, and $\sin \chi = H/H_s$. Note that both DMI components in Eqs. (19) and (20) are pointing along the out-of-plane z -axis, but the last expression (20) is no longer staggered because the sign of the Néel order on the two sublattices along the perpendicular-to-field direction cancels the staggered term ν_{ij} . As we pointed out above, the crucial point to note in this model is that the magnetic field induces two spin components parallel and perpendicular to the field. Since the DMI is a vector the magnetic field will also lead to canting which can be resolved along the in-plane and out-of-plane directions. Allowing just the latter, it is clear that the corresponding magnon dispersions cannot recover the zero magnetic field collinear Néel order with DMI because Eq. (19) will vanish at zero magnetic field. This contradicts the zero field spin Hamiltonian in Eq. (15). The point is that at low temperatures the DMI has a significant effect on the spin wave spectrum only when the magnetic order is along the same direction as the DMI. This means that in order to recover the dispersion of the collinear Néel order in the x - y plane at zero magnetic field we must include the resolution of the DMI along the in-plane direction, which would contribute to the field-induced in-plane spin components. This argument does not mean that the magnetic order determines the direction of the DMI. In fact, the main purpose of applying a magnetic field in the system is to align or cant the magnetic moments in the desired directions of the DMI (e.g. see Ref. 18). As we will show, the *magnonic DSMs* in honeycomb antiferromagnets arise from a specific field-induced spin component.

Next, we bosonize the spin operators using Eqs. (2)–(4) and Fourier transform into momentum space. In the basis $(b_{\mathbf{k},A}^{\dagger}, b_{\mathbf{k},B}^{\dagger}, b_{-\mathbf{k},A}, b_{-\mathbf{k},B})$, the momentum space Hamiltonians can be written as

$$\begin{aligned} \mathcal{H}^{\parallel}(\mathbf{k}) &= 3JSI_{\tau} \otimes I_{\sigma} + S\sqrt{v_{\chi}}d_3(\mathbf{k})\tau_z \otimes \sigma_z \\ &\quad - JSv_{\chi}I_{\tau} \otimes [\sigma_+f_{\mathbf{k}}^* + \sigma_-f_{\mathbf{k}}] \\ &\quad - JS(1 - v_{\chi})\tau_x \otimes [\sigma_+f_{\mathbf{k}}^* + \sigma_-f_{\mathbf{k}}], \end{aligned} \quad (21)$$

$$\begin{aligned} \mathcal{H}^{\perp}(\mathbf{k}) &= 3JSI_{\tau} \otimes I_{\sigma} + S\sqrt{1 - v_{\chi}}d_3(\mathbf{k})\tau_z \otimes I_{\sigma} \\ &\quad - JSv_{\chi}I_{\tau} \otimes [\sigma_+f_{\mathbf{k}}^* + \sigma_-f_{\mathbf{k}}] \\ &\quad - JS(1 - v_{\chi})\tau_x \otimes [\sigma_+f_{\mathbf{k}}^* + \sigma_-f_{\mathbf{k}}], \end{aligned} \quad (22)$$

where τ and σ are Pauli matrices acting on the $-\mathbf{k}$ and \mathbf{k} momentum spaces respectively. $\sigma_{\pm} = (\sigma_x \pm i\sigma_y)/2$ and I_{τ} and I_{σ} are 2×2 identity matrix in the τ and σ space.

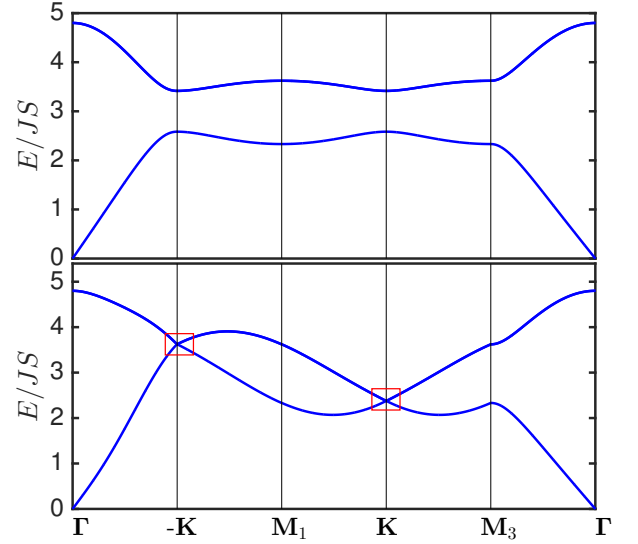


FIG. 4: Color online. Magnon band dispersions of canted Néel antiferromagnet on the honeycomb lattice. (Top) Out-of-plane spin components ($\mathbf{M} \parallel \mathbf{D} \parallel \mathbf{H}$). (Bottom) In-plane spin components ($\mathbf{M}_{st} \parallel \mathbf{D} \perp \mathbf{H}$). The rectangles indicate Dirac nodes at the high symmetry points of the Brillouin zone. They are protected by the combined symmetry $\mathcal{R}_{\pi}\mathcal{T}\mathbf{T}_{\mathbf{a}}$ and annihilate at Γ when the magnetic field vanishes or along the in-plane direction. We note that SU(2)- and U(1)-invariant interactions do not open a topological gap. The parameters for this figure are $D/J = 0.2$ and $H/H_s = 0.4$.

Here, $v_{\chi} = \sin^2 \chi$ and $f_{\mathbf{k}} = \sum_l e^{-i\mathbf{k} \cdot \delta_l}$. The magnon dispersions should be positive definite. For $0 < H < H_s$, the positive magnon dispersions are given by

$$E_{\pm}^{\parallel}(\mathbf{k}) = S\sqrt{(3J)^2 + [d^{\parallel}(\mathbf{k})]^2 - (1 - 2v_{\chi})|f_{\mathbf{k}}|^2 \pm 2\lambda_{\mathbf{k}}}, \quad (23)$$

$$\begin{aligned} E_{\pm}^{\perp}(\mathbf{k}) &= d^{\perp}(\mathbf{k}) \\ &\quad + S\sqrt{(3J)^2 - (1 - 2v_{\chi})|f_{\mathbf{k}}|^2 \pm 2(3J)v_{\chi}|f_{\mathbf{k}}|}, \end{aligned} \quad (24)$$

where $\lambda_{\mathbf{k}} = 3J\sqrt{[d^{\parallel}(\mathbf{k})]^2 + |v_{\chi}f_{\mathbf{k}}|^2}$ and $d^{\perp(\parallel)}(\mathbf{k}) = \sqrt{v_{\chi}}(\sqrt{1 - v_{\chi}})d_3(\mathbf{k})$.

The magnon bands are depicted in Fig. (4). As we can see from the dispersions, $E_{\pm}^{\parallel}(\mathbf{k})$ are the magnon dispersions of parallel-to-field spin components, which reduce to $\hat{\mathbf{z}}$ -polarized collinear ferromagnets at $H = H_s$ ($\chi = \pi/2$). On the other hand, $E_{\pm}^{\perp}(\mathbf{k})$ are the magnon dispersions of perpendicular-to-field spin components, which reduce to degenerate $\hat{\mathbf{x}}$ -antipolarized collinear Néel order at $H = 0$ ($\chi = 0$) with degenerate magnon bands, but asymmetric $E_{\mathbf{k}}^{\perp} \neq E_{-\mathbf{k}}^{\perp}$. Near $\mathbf{k} = \Gamma$ the lowest energy dispersion of both spin components is

$$E_{-}^{\perp(\parallel)}(\mathbf{k} \rightarrow \Gamma) \approx 3JS\sqrt{\frac{1}{2}(1 - v_{\chi})\mathbf{k}^2 + \frac{1}{16}v_{\chi}\mathbf{k}^4}. \quad (25)$$

In the canted Néel phase v_{χ} is small, Eq. 25 becomes a linear Goldstone mode. As we previously mentioned,

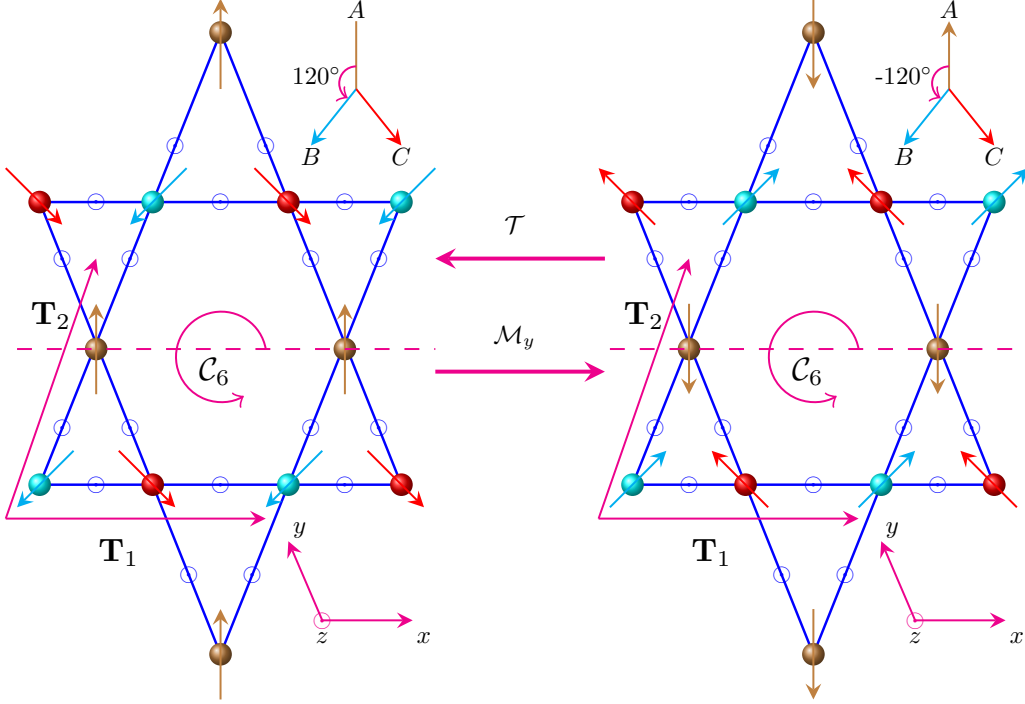


FIG. 5: Color online. The noncollinear/coplanar $\mathbf{Q} = \mathbf{0}$ magnetic order on the kagomé antiferromagnets with positive vector chirality and the associated symmetry group of the lattice. The star lattice has an additional bridge between the corner-sharing triangles coupled by J_t .

we do not identify the Goldstone mode as a Dirac node. The reason is that by definition of electronic DSMs, there should be at least two linear band crossings at the Dirac nodes. Near the ferromagnetic phase v_χ is close to unity and Eq. 25 becomes a quadratic Goldstone mode. For $\mathbf{M} \parallel \mathbf{D} \parallel \mathbf{H}$ the components of the spins along the field direction realize a topological magnon insulator for all $H \neq 0$. The existence of Dirac nodes may be possible when lattice distortion is taken into account. On the other hand, for $\mathbf{M}_{st} \parallel \mathbf{D} \perp \mathbf{H}$ the perpendicular-to-field spin components preserve $\mathcal{R}_\pi \mathcal{T} \mathbf{T}_a$ symmetry. Hence, there are Dirac nodes at $\pm \mathbf{K}$ protected by this symmetry and they cannot be removed by changing the parameters of the Hamiltonian or the magnetic field. They are robust against SU(2)- and U(1)-invariant interactions and other anisotropies. The existence of Dirac nodes for the perpendicular-to-field spin components (Néel ordered states) can be understood from Eq. 24. Expanding the dispersions in the vicinity of the Dirac points gives a linear dispersion

$$E_\pm^\perp(\tau \mathbf{K} + \mathbf{q}) = -\tau 3DS \sqrt{3(1 - v_\chi)} + 3JS(1 \pm v_s |\mathbf{q}|), \quad (26)$$

where $v_s = v_\chi/2$, $\tau = \pm$, and $\mathbf{q} = (q_x, q_y)$. Since the energy gap $\Delta_g = E_+^\perp(\mathbf{k}) - E_-^\perp(\mathbf{k})$ must vanish for linear band crossing (Dirac points) to exist, it is evident that $\Delta_g = 0$ at $\mathbf{q} = 0$. The corresponding Dirac magnon

Hamiltonian is

$$\mathcal{H}^\perp(\tau \mathbf{K} + \mathbf{q}) = [-\tau 3\sqrt{3}DS\sqrt{1 - v_\chi} + 3JS]I_\sigma + 3JSv_s(\sigma_x q_x + \sigma_y q_y). \quad (27)$$

The topological protection of Dirac nodes is related to a Berry phase [76] defined as

$$\gamma = \oint_{\mathcal{C}} \mathcal{A}(\mathbf{q}) \cdot d\mathbf{q}, \quad (28)$$

where $\mathcal{A}(\mathbf{q})$ is the Berry connection given by $\mathcal{A}(\mathbf{q}) = i \langle \psi_{\mathbf{q}} | \vec{\nabla}_{\mathbf{q}} \psi_{\mathbf{q}} \rangle$. If \mathcal{C} encircles the Dirac nodes in momentum space we have $\gamma = \pm\pi$, otherwise $\gamma = 0$, just like in graphene.

IV. FRUSTRATED MAGNETS

A. Model

In this section, we study non-bipartite frustrated magnets, where there is no long-range magnetic order down to lowest temperatures and the classical ground states have an extensive degeneracy. These frustrated magnets are considered as candidates for quantum spin liquids (QSLs) [74, 75]. However, QSL materials are elusive experimentally because the effects of SOI or DMI

are not negligible in frustrated magnets. The DMI is intrinsic to the kagomé and star lattices and it can induce a non-collinear long-range magnetic order with a $\mathbf{Q} = \mathbf{0}$ propagation vector with the spins oriented at 120° apart [77] (see Fig. 5). In other words, the DMI suppresses the QSL phase in frustrated magnets up to a quantum critical point for spin-1/2 systems [78]. Apart from the DMI, a second nearest-neighbour antiferromagnetic interaction can equally induce a non-collinear long-range magnetic order in frustrated magnets [79]. Therefore, many frustrated magnets actually show evidence of coplanar/noncollinear $\mathbf{Q} = \mathbf{0}$ long-range magnetic order at specific temperatures [58–62].

The minimal spin Hamiltonian for kagomé antiferromagnets is given by

$$\mathcal{H} = J \sum_{\langle ij \rangle} \mathbf{S}_i \cdot \mathbf{S}_j + \sum_{\langle ij \rangle} \mathbf{D}_{ij} \cdot \mathbf{S}_i \times \mathbf{S}_j, \quad (29)$$

where J is the nearest-neighbour antiferromagnetic interaction. The DM vector \mathbf{D}_{ij} in this case is allowed on the nearest-neighbour bonds between sites i and j within the triangular plaquettes. The DMI usually points perpendicular to the plane of the magnet (out-of-plane) $\mathbf{D}_{ij} = \pm D \hat{\mathbf{z}}$, where \pm alternates between down and up pointing triangles of the lattice respectively [77]. The sign of the DMI determines the vector chirality of the 120° order. The out-of-plane DMI breaks $SU(2)$ rotational symmetry down to $U(1)$ symmetry about the z -axis. But it preserves translational and \mathcal{C}_6 (i.e $\pi/3$ rotation about the z -axis through the hexagonal plaquettes) crystal symmetries as shown in Fig. 5. The out-of-plane DMI also preserves mirror reflection (\mathcal{M}) symmetry of the kagomé lattice.

B. Intrinsic magnonic Dirac semimetal

We note that tunable electronic DSMs are usually difficult to achieve experimentally because they require the manipulation of the chemical composition of the materials. However, intrinsic electronic DSMs do not require any tunable parameters and they are of importance and they can occur away from the high symmetry points of the BZ and require additional crystal symmetries [8–10]. As we showed above, the magnetic field induces the spin components that possess the Dirac points in honeycomb antiferromagnets. In the distorted quantum ferromagnets there is no Dirac point without lattice distortion i.e. $J_{ij} = J$, due to the DMI. Hence the lattice distortion which can be achieved by applying a strain induces a Dirac point in the presence of DMI. Thus, a natural question that arises is: can an intrinsic *magnonic DSM* exist in quantum magnets without any external effects? The purpose of this section is to show that intrinsic *magnonic DSMs* can be realized in quasi-2D quantum antiferromagnets on non-bipartite frustrated magnets. As we hinted above the DMI is intrinsic to the kagomé and star lattices

and it can induce a non-collinear $\mathbf{Q} = \mathbf{0}$ long-range magnetic order in frustrated non-bipartite quantum magnets, whereas it induces topological magnon bands in collinear unfrustrated non-bipartite magnets such as the collinear ferromagnets on the pyrochlore, kagomé, and star lattices [19, 23, 25].

For the frustrated kagomé-lattice and star-lattice magnets, the magnon bands of non-collinear $\mathbf{Q} = \mathbf{0}$ long-range magnetic order have an *effective time-reversal symmetry* even though \mathcal{T} -symmetry has been broken by the long-range magnetic order. For instance, the mirror reflection symmetry \mathcal{M}_y with respect to the kagomé plane is a good symmetry of the kagomé lattice as well as the star lattice. For a perfect kagomé or star lattice \mathcal{M}_y -symmetry is present, which forbids an in-plane DMI according to the Moriya rules [42]. However, \mathcal{M}_y -symmetry flips the in-plane $\mathbf{Q} = \mathbf{0}$ magnetic order and \mathcal{T} -symmetry flips the magnetic order the second time, hence the *effective time-reversal symmetry* $\mathcal{T}\mathcal{M}_y$ is a good symmetry of the non-collinear $\mathbf{Q} = \mathbf{0}$ magnetic order as shown in Fig. 5. However, this *effective time-reversal symmetry* does not guarantee doubly degenerate magnon bands for the non-collinear $\mathbf{Q} = \mathbf{0}$ magnetic order as one would expect in electronic systems. Rather, it supplies a *magnonic DSM* as we now show in the following. We take the spins to lie on the plane of the magnets taken as the x - y plane as shown in Fig. 5. Then, we perform a rotation about the z -axis on the sublattices by the spin oriented angles, say θ_i , in order to achieve the 120° magnetic order (see Fig. 5).

$$S_i^x = S_i'^x \cos \theta_i - S_i'^y \sin \theta_i, \quad (30)$$

$$S_i^y = S_i'^x \sin \theta_i + S_i'^y \cos \theta_i \quad (31)$$

$$S_i^z = S_i'^z. \quad (32)$$

The corresponding Hamiltonian that contributes to non-interacting magnon tight binding model is given by

$$\mathcal{H}_J = J \sum_{\langle ij \rangle} [\cos \theta_{ij} (S_i'^x S_j'^x + S_i'^y S_j'^y) + S_i'^z S_j'^z], \quad (33)$$

$$\mathcal{H}_{DMI} = D \sum_{\langle ij \rangle} \sin \theta_{ij} (S_i'^x S_j'^y - S_i'^y S_j'^x), \quad (34)$$

where $\theta_{ij} = \theta_i - \theta_j$. The alternating DMI selects only one ground state for each sign with $D > 0$ (positive vector chirality ground state) and $D < 0$ (negative vector chirality ground state) (see Ref.[77]). We have taken the former case shown in Fig. 5. The appropriate HP spin-boson transformations are given by

$$S_{i,\alpha}^{y'} = S - b_{i,\alpha}^\dagger b_{i,\alpha}, \quad (35)$$

$$S_{i,\alpha}^{x'} = \sqrt{\frac{S}{2}} (b_{i,\alpha}^\dagger + b_{i,\alpha}), \quad (36)$$

$$S_{i,\alpha}^{z'} = i\sqrt{\frac{S}{2}} (b_{i,\alpha}^\dagger - b_{i,\alpha}). \quad (37)$$

In stark contrast to ferromagnets and bipartite antiferromagnets, it is evident that no imaginary hopping term

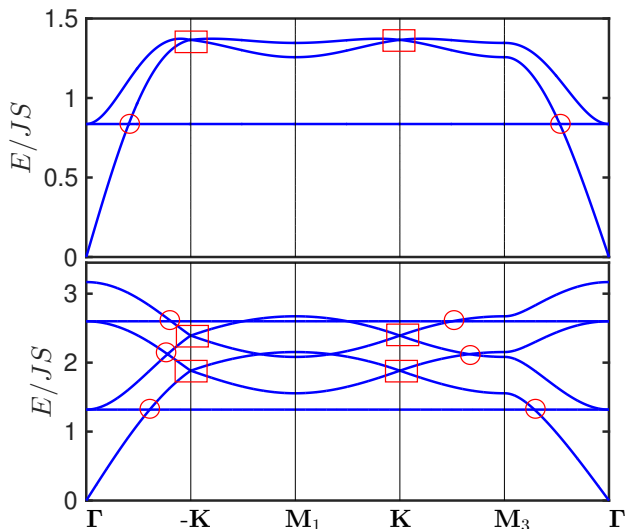


FIG. 6: Color online. Magnon band dispersions of non-collinear $\mathbf{Q} = \mathbf{0}$ long-range magnetic order in frustrated magnets. (Top) Kagomé lattice. (Bottom) Star lattice. The rectangles indicate Dirac nodes at the high symmetry points and the circles form closed line of Dirac nodes away from the high symmetry points. We note that SU(2)- and U(1)-invariant interactions do not open a topological gap. The parameters for this figure are $D/J = 0.2$ and $J_t/J = 1.5$ for the star lattice inter-triangle coupling.

is possible in \mathcal{H}_{DMI} . Therefore we expect that this system will not have Chern number protected topological magnon bands.

The magnon energy bands for the kagomé- and star-lattice antiferromagnets are shown in Fig. 6 with only isotropic nearest neighbour interactions and finite DMI. The BZ has the same shape as the honeycomb lattice. For the star lattice there is an additional spin interaction J_t connecting up and down pointing triangles of the lattice [65]. The magnon dispersions have flat modes which correspond to lifted zero energy modes due to the DMI. As expected from the above analysis, the DMI or SOI is unable to gap the Dirac magnon at $\pm\mathbf{K}$, hence we obtain an intrinsic *magnonic DSM* without any tunable quantity. The energy of two magnon dispersions near the crossing points has a linear form

$$E_{\pm}(\tau\mathbf{K} + \mathbf{q}) = f_0 \pm f_1|\mathbf{q}|, \quad (38)$$

where

$$f_0 = JS\sqrt{\frac{3}{2}(1 + D_J)}, \quad (39)$$

$$f_1 = \frac{DS}{2}\sqrt{\frac{1 + D_J}{2}}, \quad (40)$$

$\mathbf{K} = (2\pi/3, 0)$ and $D_J = D/J$. The projection of the Hamiltonian onto the crossing magnon bands gives a two-dimensional (2D) Dirac Hamiltonian

$$\mathcal{H}(\tau\mathbf{K} + \mathbf{q}) = f_0\mathbb{I}_{2\times 2} + f_1(\tau q_x\sigma_x + q_y\sigma_y). \quad (41)$$

For a closed loop encircling the Dirac magnon points at $\pm\mathbf{K}$, the winding numbers are $\gamma/\pi = \pm 1$ which signify a topological vortex. Realistic materials may possess a second nearest-neighbour antiferromagnetic interaction, but since it is SU(2)-invariant and breaks no symmetry it will have no effect on the Dirac nodes. However, it gives the flat magnon bands a small dispersion [63], but does not open a topological gap (not shown).

C. Effects of broken symmetry

Now, if the mirror reflection symmetry of the lattice is broken on the kagomé-lattice and star-lattice antiferromagnets, a small in-plane DM component will be allowed. This DM component can lead to weak out-of-plane ferromagnetism with a small ferromagnetic moment. It could in some cases generate spin canting with finite scalar spin chirality if the in-plane DM component is the dominant anisotropy [80]. Therefore, the protected symmetry of the Dirac nodes \mathcal{TM}_y will be broken by the weak ferromagnetism and a small gap will open at the Dirac nodes with potential topological features. However, many frustrated kagomé antiferromagnets have dominant intrinsic out-of-plane DMI. In this case, the small in-plane DM components and the associated scalar spin chirality will be negligible. To generate a topological phase in this scenario will require an extrinsic perturbation similar to DSM in electronic systems [9]. One possibility is to apply a Zeeman magnetic field in the $\mathbf{Q} = \mathbf{0}$ magnetic order perpendicular the lattice plane. For iron jarosites the magnetic field can induce a phase transition to a state with finite scalar spin chirality [64], which breaks \mathcal{T} -symmetry macroscopically. Hence, the combined symmetry \mathcal{TM}_y is broken. An out-of-plane magnetic field can equally induce scalar spin chirality due to non-coplanar spin texture even in the absence of an explicit DMI; this leads to topological magnon bands and Chern number protected magnon edge modes with finite thermal Hall effect as recently proposed theoretically [81, 82].

V. CHIRAL MAGNON EDGE MODES

Thus far, we have studied only the existence of Dirac nodes in quantum magnets with non-negligible DMI. In principle, there exists nearly flat chiral edge modes which connect the two Dirac nodes with opposite chirality. In this section, we present the chiral edge modes of the quasi-2D quantum magnetic systems studied above. First we consider the topological phase transition of the distorted honeycomb ferromagnets studied in Sec. II B. In Fig. 7, we have shown the evolution of the bulk magnon bands using a zig-zag strip geometry for several values of J_2 at $J' = 0$. In the regime $J_2 < J_2^c$ there are gapless magnon edge modes as expected in a topological magnon system. The bulk magnon bands closes at the phase boundary $J_2 = J_2^c$ and the edge modes are suppressed.

This signifies a topological magnon phase transition. On the other hand, for $J_2 > J_2^c$ the bulk magnon bands are gapped, however no magnon edge modes are observed in the vicinity of the bulk magnon gap. This phase exhibits the characteristics of a “trivial magnon insulator phase”. As we will show below this trivial magnon insulator phase is different from those without DMI in that it can possess a finite thermal Hall conductivity in stark contrast to electronic systems.

We characterize these magnon phases using the Chern number given by

$$\mathcal{C}_\alpha = \frac{1}{2\pi} \int_{BZ} dk_i dk_j \Omega_{ij;\alpha}(\mathbf{k}). \quad (42)$$

The Berry curvature is given by

$$\Omega_{ij;\alpha}(\mathbf{k}) = - \sum_{\alpha' \neq \alpha} \frac{2\text{Im}[\langle \mathcal{U}_{\mathbf{k}\alpha} | v_i | \mathcal{U}_{\mathbf{k}\alpha'} \rangle \langle \mathcal{U}_{\mathbf{k}\alpha'} | v_j | \mathcal{U}_{\mathbf{k}\alpha} \rangle]}{(E_{\mathbf{k}\alpha} - E_{\mathbf{k}\alpha'})^2}, \quad (43)$$

where $v_i = \partial \mathcal{H}(\mathbf{k}) / \partial k_i$ defines the velocity operators with $i, j = x, y$, and $\mathcal{U}_{\mathbf{k}\alpha}$ are the eigenvectors. This formula also applies to antiferromagnetic systems in which the eigenvectors are columns of a paraunitary operator that diagonalizes the spin wave Hamiltonian. It can be reduced to a compact form for systems with simple eigenvectors. To substantiate the topological distinctions studied in Sec. IIB, we have computed the Chern number across the phase boundary and find that in the topological insulator regime ($J_2 < J_2^c$) the gapless magnon edge modes are protected by Chern numbers $\mathcal{C}_\pm = \pm 1$ for the upper and lower bands respectively, whereas the regime of trivial magnon insulator ($J_2 > J_2^c$) has vanishing Chern numbers. This sign change in the Chern number is a solid evidence of a topological magnon phase transition. The same situation is observed for $J' \neq 0$ across the phase boundary.

Now, we consider the field-induced and intrinsic *magnonic DSMs* studied in Secs. IIIB and IVB. In Fig. 8 we have shown the chiral magnon edge modes of the canted Néel order in honeycomb antiferromagnets in Sec. IIIB. For the parallel spin components $\mathbf{M} \parallel \mathbf{D} \parallel \mathbf{H}$ the system is a topological magnon insulator with gapless magnon edge modes protected by $\mathcal{C}_\pm = \pm 1$. For the perpendicular spin components with $\mathbf{M}_{st} \parallel \mathbf{D} \perp \mathbf{H}$ there are Dirac nodes at finite energy for all field values and a single edge mode connects the bulk Dirac magnon cones. They are protected by the combined symmetry $\mathcal{R}_\pi \mathcal{T} \mathbf{T}_a$ and can be manipulated by the magnetic field. The magnon edge modes for non-collinear $\mathbf{Q} = \mathbf{0}$ magnetic order in Sec. IVB are shown in Fig. 9. In this case the system is an intrinsic *magnonic DSMs* and a single edge mode connects the bulk Dirac magnon cones. They are also protected by the combined symmetry $\mathcal{T} \mathcal{M}_y$. As shown above, the *magnonic DSMs* are characterized by opposite Berry flux or winding numbers [76] of $\gamma/\pi = \pm 1$ defined around a closed loop encircling the Dirac nodes. This is related to the Chern numbers of a topological gap system.

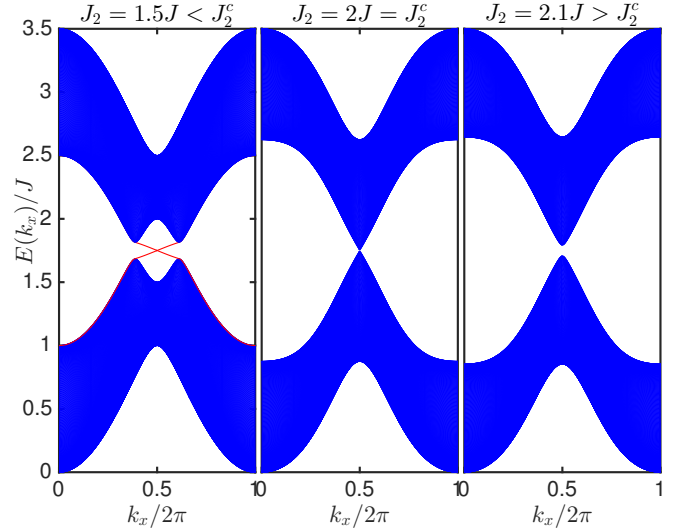


FIG. 7: Color online. Chiral edge modes (red lines) and topological phase transition in the distorted honeycomb ferromagnets with a zig-zag strip geometry at $J' = 0$, $D/J = 0.2$ and several values of J_2 .

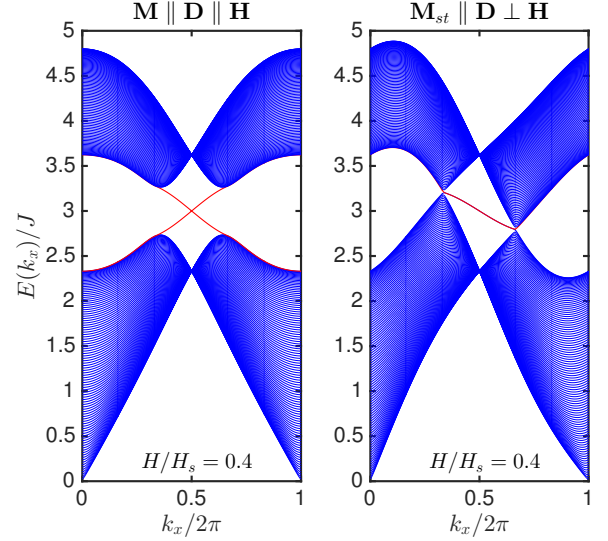


FIG. 8: Color online. Chiral edge modes (red lines) of canted Néel order for out-of-plane spin components (left) and in-plane spin components (right) for a zig-zag strip at $D/J = 0.2$.

VI. EXPERIMENTAL REALIZATIONS

A. Thermal Hall Response

One of the recent exciting experimental probes in quantum magnetism is the measurement of thermal Hall conductivity and topological magnon bands [15–18]. Although magnons are charge-neutral quasiparticles that do not experience a Lorentz force, a temperature gradi-

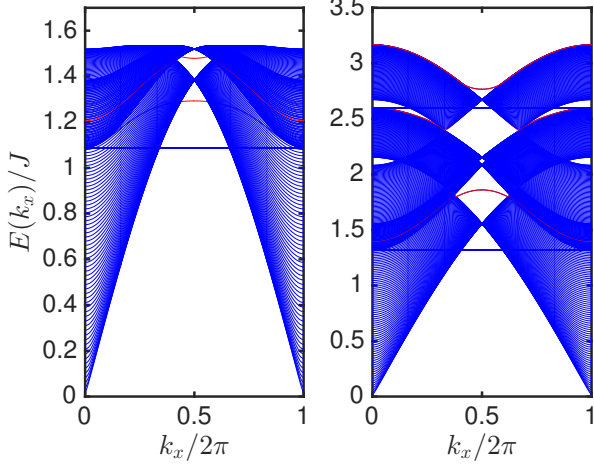


FIG. 9: Color online. Magnon edge modes (red lines) of non-collinear $\mathbf{Q} = \mathbf{0}$ magnetic order in frustrated kagomé (left) and star (right) lattices with a zig-zag strip geometry. The parameters for this figure are $D/J = 0.2$ and $J_t/J = 1.5$ for the star lattice inter-triangle coupling.

ent $-\nabla T$ can induce a heat current \mathcal{J}^Q and the Berry curvature induced by the DMI acts as an effective magnetic field in momentum space that deflects the propagation of the spin excitations in the system [17–20, 22–25, 27, 28]. This leads to a thermal analog of quantum anomalous Hall effect. From linear response theory, one obtains $\mathcal{J}_\alpha^Q = -\sum_\beta \kappa_{\alpha\beta} \nabla_\beta T$, where $\kappa_{\alpha\beta}$ is the thermal conductivity and the transverse component κ_{xy} is associated with the thermal Hall conductivity given explicitly as [20, 24]

$$\kappa_{xy} = -k_B^2 T \int_{BZ} \frac{d^2 k}{(2\pi)^2} \sum_{\alpha=1}^N c_2(n_\alpha) \Omega_{\alpha\mathbf{k}}, \quad (44)$$

where k_B is the Boltzmann constant, T is the temperature, $n_\alpha = n(E_{\alpha\mathbf{k}}) = (e^{E_{\alpha\mathbf{k}}/k_B T} - 1)^{-1}$, is the Bose function and $c_2(x) = (1+x)(\ln \frac{1+x}{x})^2 - (\ln x)^2 - 2\text{Li}_2(-x)$, with $\text{Li}_2(x)$ being the dilogarithm.

The purpose of this section is to show that the thermal Hall conductivity can be present in the absence of magnon edge modes and Chern numbers. In other words, the trivial magnon insulator phase in the distorted honeycomb ferromagnets will possess a finite nonzero value of κ_{xy} , despite the absence of magnon edge modes and Chern numbers. This is in contrast to electronic systems where the Fermi energy can guarantee a completely filled band and vanishing Hall conductivity in the trivial insulator phase, but in magnonic (bosonic) systems this is not possible due to the Bose distribution function. Therefore, thermal Hall effect in quantum magnets is not directly connected to Chern number protected bands.

Using Eq. 44, we compute the transverse thermal Hall conductivity for the distorted honeycomb ferromagnetic model. As shown in Fig. 10 the Hall conductivity is fi-

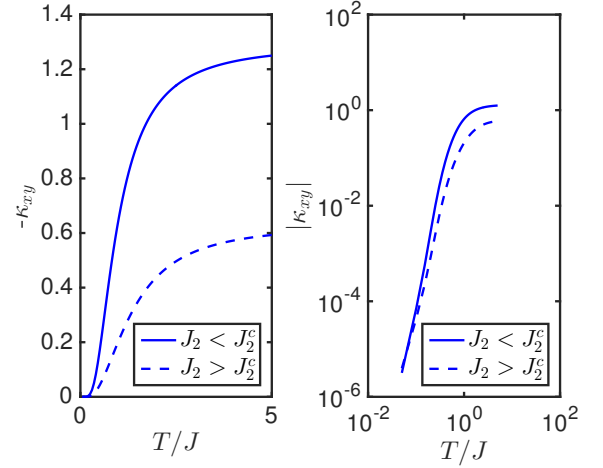


FIG. 10: Color online. (Left). κ_{xy} vs. T . (Right). Log-log plot of $|\kappa_{xy}|$ vs. T . The topological ($J_2 = 1.5J < J_2^c$) and trivial insulators ($J_2 = 2.1J > J_2^c$) are distinguished at $D/J = 0.2$ and $J' = 0$.

nite in both the topological and trivial insulator regimes of the system as mentioned above. We also see that κ_{xy} is suppressed in the trivial insulator phase. It has also been confirmed that the inclusion of a third nearest neighbour suppresses κ_{xy} in each regime. The Hall conductivity is negative and never changes sign because the Chern number of the bulk bands is either $|\mathcal{C}_\pm| = 1$ in the topological regime or $|\mathcal{C}_\pm| = 0$ in the trivial insulating regime. At low temperatures the lower band is more populated at $\mathbf{k} = 0$ (Bose condensation) than the upper band and the Berry curvature can be expanded near $\mathbf{k} = 0$. The resulting Hall conductivity in the low temperature regime follows a power-law as shown using log-log plot in Fig. 10 (right), that is $|\kappa_{xy}| \propto T^a$ where $a = 2$ in the present model. The conductivity can also be computed for the parallel-to-field spin components of honeycomb antiferromagnets as they form a topological magnon insulator.

In the *magnonic DSMs* which are manifested from the perpendicular-to-field spin components on the honeycomb antiferromagnets and the coplanar/noncollinear $\mathbf{Q} = \mathbf{0}$ long-range magnetic order in frustrated antiferromagnets, the thermal Hall conductivity vanishes due to symmetry. As we previously mentioned, every ordered quantum magnetic system will not break \mathcal{T} -symmetry macroscopically even in the presence of DMI, therefore Dirac magnon nodes will inevitably be present in the Brillouin zone of these systems and the Berry curvature will vanish by symmetry. However, due to the 3D nature of WMs [43, 44] the Berry curvature is nonzero and there is a finite thermal Hall conductivity [15, 16]. It is tempting to say that the nomenclatures *WMs* and *magnonic DSMs* with finite DMI can be used to characterize 2D and 3D magnetic systems with long-range magnetic orders based on whether they possess a thermal Hall effect or not.

B. Bose Gas in Optical Lattice

The bosonic nature of quantum magnetic excitations makes optical lattices an indispensable reliable medium to experimentally probe nontrivial properties of these systems [84–93]. The optical lattice mechanism has been utilized effectively in the realization of artificial vector gauge potential for neutral bosonic particles trapped in an optical lattice [89, 90]. Therefore, it is possible to generate fictitious magnon phases by trapping ferromagnetic magnon or Bose atoms in an optical lattice [86] as implemented in the electronic version of Haldane model [94]. The simplicity of this model makes these approaches very promising. To realize bosonic cold atoms in this model, it is worth pointing out that the connection between spin-1/2 quantum magnets and bosonic systems can be achieved via the Matsubara-Matsuda transformation $S_i^+ \rightarrow a_i^\dagger$, $S_i^- \rightarrow a_i$, $S_i^z = a_i^\dagger a_i - 1/2$ [95], where $S^\pm = S^x \pm iS^y$, a_i^\dagger and a_i are the bosonic creation and annihilation operators respectively. The bosonic operators obey the algebra $[a_i, a_j^\dagger] = 0$ for $i \neq j$ and $\{a_i, a_i^\dagger\} = 1$. The resulting bosonic Hamiltonian for the honeycomb ferromagnets is given by

$$\begin{aligned} \mathcal{H} = & - \sum_{\langle ij \rangle} t_{ij} (a_i^\dagger a_j + h.c.) - t' \sum_{\langle\langle ij \rangle\rangle} (e^{i\nu_{ij}\phi} a_i^\dagger a_j + h.c.) \\ & + (U + U_d) \sum_{\langle ij \rangle} \left(n_i - \frac{1}{2} \right) \left(n_j - \frac{1}{2} \right) - \mu \sum_i n_i, \quad (45) \end{aligned}$$

where $n_i = a_i^\dagger a_i$, $t_{ij} \rightarrow J_{ij}/2$, $\mu \rightarrow H$, $t' \rightarrow -D/2$, $U \rightarrow -J$, $U_d \rightarrow -J_2$, and $\phi = \pi/2$. This model is the bosonic version of the magnonic system in Eq. 1 and it represents a system of Bose gas interacting via a potential [96]. In this system the topological magnon phase for $J_2 < J_2^c$ can be attributed to a topological superfluid phase, whereas the trivial magnon insulator phase for $J_2 > J_2^c$ could be a non-topological Mott phase and the critical point $J_2 = J_2^c$ is the topological phase transition. A superfluid-Mott insulator transition has been previously realized in a non-topological bosonic optical lattice [91, 93]. Thus, the present model can be designed in a gas of ultracold bosonic atoms at sufficiently low temperatures [84, 85, 87, 88], and distortion can be created by anisotropic laser-beam potentials. An alternative model with similar phase transition is the hardcore-Bose-Hubbard model on the honeycomb lattice [97] which maps to Heisenberg XY model with uniform and staggered magnetic fields [98].

VII. DISCUSSION

It is important to point out that the nomenclature *magnonic DSM* does not obey the true meaning of semimetals in electronic systems in terms of the conduction and valence band touching. However, the concepts

of linear band touching (crossing) points, Berry curvature, and Chern number are independent of the statistical nature of the particles. We remind the reader that *magnonic DSMs* in quantum magnetism with DMI are different from Dirac magnons in the conventional quantum magnets without DMI. It is well-known in electronic systems that in the absence of SOI a DSM cannot be driven to any topological phase by an external perturbation. This is also true in quantum magnets with SOI replaced by the DMI. For instance, the Dirac magnons in the conventional ferromagnetic systems on the honeycomb lattice without DMI [66] cannot be driven to a topological magnon phase by an external perturbation due to the coexistence of time-reversal and inversion symmetry of the lattice.

The DMI in quantum magnets is intrinsic to the magnetic materials. It usually breaks the time-reversal symmetry of the associated magnon bands. We therefore expect a topological magnon insulator [22, 23]. The presence of Dirac magnon nodes in magnetic systems that are expected to be topological (i.e. with finite DMI) has never been studied. This is the main result of this Communication and they are present due to an *effective time-reversal symmetry* (i.e. time-reversal + crystalline symmetries such mirror symmetry, lattice translation, and rotation symmetry). They can also be driven to a topological magnon phase by an external perturbation that breaks the *effective time-reversal symmetry*.

Another crucial distinguishing feature of magnetic insulators with DMI is that the topological and trivial insulator phases possess a finite transport property such as the thermal Hall effect, despite the absence of Chern number protected edge modes in the latter. This shows that, in contrast to previous studies, magnon edge modes and Chern numbers are not directly connected with thermal Hall conductivity. In other words, strong SO coupling magnetic insulators without Chern number protected magnon bands can also possess a thermal Hall effect. As we mentioned above, this is not possible in the conventional (trivial) ferromagnetic systems without DMI and it is also in stark contrast to electronic systems. We note that the Dirac magnon nodes at the topological phase transition between topological and trivial magnon insulators are not robust as they depend on the critical value of the interactions, which is usually not very easy to achieve experimentally. A robust *magnonic DSMs* does not necessarily require any tunable parameters as in the case of the $\mathbf{Q} = \mathbf{0}$ long-range magnetic order in frustrated magnets.

It is important to mention that the magnonic analogs of electronic topological systems are not exactly the same as the original electronic systems. For instance, topological magnon insulators break time-reversal symmetry, whereas electronic topological insulators preserve time-reversal symmetry. One of the differences comes from the fact that the former is a localized spin magnet with bosonic spin-1 dispersions and the latter is an itinerant magnet with spin-1/2 electronic dispersions. The spin-

1/2 electrons with SOI preserves time-reversal symmetry and by the Kramers' theorem the system should have at least doubly degenerate bands. On the other hand, the localized spin magnets with DMI breaks time-reversal symmetry and the analog of Kramers' degeneracy is not directly obvious. However, both interactions can lead to a topological band insulator with similar properties. In other words, one can regard the DMI in magnetic insulators as a single copy of SOI in electronic systems. We remind the reader that the DMI arises as the leading order term in the perturbative expansion of the SOI, hence it is plausible that the DMI does not retain the full symmetry of SOI.

We would also like to point out to the reader that WMs differ from *magnonic DSMs*. One of the major differences is the presence or absence of an *effective time-reversal symmetry* in magnetic systems with long-range orders. In the ferromagnetic systems (such as the pyrochlore and kagomé lattice), the spontaneous magnetization combined with the DMI breaks time-reversal symmetry macroscopically. Hence, the WMs in pyrochlore ferromagnets with DMI [15, 16] have a direct analog to electronic Weyl semimetals with broken time-reversal symmetry. On the other hand, in the antiferromagnetic systems with long-range magnetic order and finite DMI, the Dirac nodes are protected by an *effective time-reversal symmetry*, which gives an *indirect*¹² analog of electronic DSMs. However, the electronic and magnonic DSMs are directly analogous in that both systems have Dirac nodes unaffected by SOI or DMI and they can be driven to a topological band insulator by introducing a mass term through symmetry breaking by external perturbations.

VIII. CONCLUSION

In quantum magnetic systems that lack an inversion center the Dzyaloshinskii-Moriya interaction (DMI) is present. In this Communication, we have shown that quasi-two-dimensional (quasi-2D) magnetic systems with collinear and non-collinear long-range magnetic order exhibit gapless cone-like Dirac magnon dispersions unaffected by the DMI. They are dubbed *magnonic DSMs* and they occur in magnetic systems with at least two magnon energy branches. We also noted that not all linear dispersions form Dirac nodes in quantum magnetic systems. For instance, antiferromagnetic systems (topological or trivial insulators) usually have a linear Goldstone mode dispersion in the limit of $\mathbf{k} \rightarrow 0$, but this is not a Dirac node formed by two-band crossing as the

negative energy solution has no physical meaning. The possibility of Dirac cone dispersions can be probed by inelastic neutron scattering [18].

We remark that the simplest realistic method to observe *magnonic DSMs* is by regulating the magnetic moments using an external magnetic field. Indeed, when the magnetic moments are perpendicular to the DMI no gap opens in the magnon dispersions. For example, the kagomé ferromagnet Cu(1,3-bdc) with small interlayer coupling [18] has its magnetic moments perpendicular to the DMI at zero magnetic field and they remain the same in the presence of an in-plane magnetic field. In this scenario the out-of-plane DMI is unable to open a gap between the magnon bands [18]. In principle, an in-plane DMI would contribute to the in-plane magnetic moments and it might open a gap, however no sizeable in-plane DMI was observed in Cu(1,3-bdc), only an out-of-plane DMI ($D/J = 0.15$) was observed [18]. The spin-1/2 kagomé ferromagnetic mineral haydeeite, α - $\text{MgCu}_3(\text{OD})_6\text{Cl}_2$, also shows no finite-energy gaps in the observed spin-wave spectra [57]. It was suggested that the DMI does not play a significant role in haydeeite. But it is possible that the magnetic moments are perpendicular to the DMI, which leads to unavoidable band crossing in the spin wave spectra. Hence, one might conclude that the DMI does not break time-reversal symmetry of the magnon dispersions macroscopically when the magnetic moments are perpendicular to the DMI. As shown above a similar effect is manifested on the honeycomb antiferromagnets where the in-plane spin components show gapless magnon bands protected by the coexistence of time-reversal symmetry and lattice translations.

In frustrated magnets, *magnonic DSMs* are intrinsic since the out-of-plane DMI is always perpendicular to the in-plane $\mathbf{Q} = \mathbf{0}$ magnetic order in the absence of any external effects such as the magnetic field. In the presence of mirror reflection symmetry, a linear unavoidable magnon band crossing will be present in the spin wave spectra. It would be interesting to re-examine the spin-wave spectra of the materials mentioned in the Introduction in the new context of *magnonic DSMs*. Since the long-range magnetic orders in these magnetic materials occur at finite temperatures, an experimental scan of the spin-wave spectra at various magnetic field and temperature ranges will provide a complete topological magnon phase transition. The chiral edge modes should provide magnon transport on the edge of the materials, however they have not been measured at the moment. They require edge sensitive methods such as light [99] or electronic [100] scattering method. These systems can also be realized in optical lattices by trapping magnons or Bose gases in laser beam potentials.

Acknowledgments

Research at Perimeter Institute is supported by the Government of Canada through Industry Canada and by

¹ It is indirect in the sense that the effective time-reversal symmetry does not give Kramers degenerate bands as mentioned above

² In fact, broken time-reversal symmetry by the magnetic order removes spin degenerate

-
- [1] F. D. M. Haldane, Phys. Rev. Lett. **61**, 2015 (1988).
- [2] C.L. Kane and E.J. Mele, Phys. Rev. Lett. **95**, 146802 (2005).
- [3] Xiao-Liang Qi and Shou-Cheng Zhang, Rev. Mod. Phys. **83**, 1057 (2011).
- [4] M. Z. Hasan and C. L. Kane, Rev. Mod. Phys. **82**, 3045 (2010).
- [5] Shuichi Murakami, Satoshi Iso, Yshai Avishai, Masaru Onoda, Naoto Nagaosa, Phys. Rev. B **76**, 205304 (2007).
- [6] Thomas C. Lang, Andrew M. Essin, Victor Gurarie, Stefan Wessel, Phys. Rev. B **87**, 205101 (2013).
- [7] Steve M. Young and Charles L. Kane, Phys. Rev. Lett. **115**, 126803 (2015).
- [8] S. M. Young, S. Zaheer, J. C. Y. Teo, C. L. Kane, E. J. Mele, and A. M. Rappe, Phys. Rev. Lett. **108**, 140405 (2012).
- [9] Zhijun Wang, Yan Sun, Xing-Qiu Chen, Cesare Franchini, Gang Xu, Hongming Weng, Xi Dai, and Zhong Fang, Phys. Rev. B **85**, 195320 (2012).
- [10] Sergey Borisenko, Quinn Gibson, Danil Evtushinsky, Volodymyr Zabolotnyy, Bernd Büchner, and Robert J. Cava, Phys. Rev. Lett. **113**, 027603 (2014).
- [11] X. Wan, A. M. Turner, A. Vishwanath, and S. Y. Savrasov, Phys. Rev. B **83**, 205101 (2011).
- [12] L. Balents, Physics **4**, 36 (2011).
- [13] A. A. Burkov and L. Balents, Phys. Rev. Lett. **107**, 127205 (2011).
- [14] S. A. Owerre, J. Phys.: Condens. Matter **28**, 235501 (2016).
- [15] Y. Onose, T. Ideue, H. Katsura, Y. Shiomi, N. Nagaosa, Y. Tokura, Science **329**, 297 (2010).
- [16] T. Ideue, Y. Onose, H. Katsura, Y. Shiomi, S. Ishiwata, N. Nagaosa, and Y. Tokura, Phys. Rev. B **85**, 134411 (2012).
- [17] Max Hirschberger, Robin Chisnell, Young S. Lee, and N. P. Ong, Phys. Rev. Lett. **115**, 106603 (2015).
- [18] R. Chisnell, J. S. Helton, D. E. Freedman, D. K. Singh, R. I. Bewley, D. G. Nocera, and Y. S. Lee, Phys. Rev. Lett. **115**, 147201 (2015).
- [19] H. Katsura, N. Nagaosa, and P. A. Lee, Phys. Rev. Lett. **104**, 066403 (2010).
- [20] R. Matsumoto and S. Murakami, Phys. Rev. Lett. **106**, 197202 (2011); Phys. Rev. B **84**, 184406 (2011).
- [21] Ryuichi Shindou, Ryo Matsumoto, Shuichi Murakami, and Jun-ichiro Ohe, Phys. Rev. B **87**, 174427 (2013).
- [22] L. Zhang, J. Ren, J. S. Wang, and B. Li, Phys. Rev. B **87**, 144101 (2013).
- [23] A. Mook, J. Henk, and I. Mertig, Phys. Rev. B **90**, 024412 (2014); *ibid*, Phys. Rev. B **89**, 134409 (2014).
- [24] R. Matsumoto, R. Shindou, and S. Murakami, Phys. Rev. B **89**, 054420 (2014).
- [25] H. Lee, J. H. Han, and P. A. Lee, Phys. Rev. B **91**, 125413 (2015).
- [26] X. Cao, K. Chen, and D. He, J. Phys.: Condens. Matter **27**, 166003 (2015).
- [27] S. A. Owerre, J. Phys.: Condens. Matter **28**, 386001 (2016).
- [28] S. A. Owerre, J. Appl. Phys. **120**, 043903 (2016).
- [29] Se Kwon Kim, Héctor Ochoa, Ricardo Zarzuela, Yaroslav Tserkovnyak, Phys. Rev. Lett. **117**, 227201 (2016).
- [30] A Roldán-Molina, A S Nunez, and J Fernández-Rossier, New J. Phys. **18**, 045015 (2016).
- [31] Emil Prodan and Camelia Prodan, Phys. Rev. Lett. **103**, 248101 (2009).
- [32] L. Zhang, J. Ren, J.-S. Wang, and B. Li, Phys. Rev. Lett. **105**, 225901 (2010).
- [33] L. Zhang, J. Ren, J.-S. Wang, and B. Li, J. Phys. Condens. Matter **23**, 305402 (2011).
- [34] T. Qin, J. Zhou, and J. Shi, Phys. Rev. B **86**, 104305 (2012).
- [35] C. Kane and T. C. Lubensky, Nat. Phys. **10**, 39 (2014).
- [36] J. Paulose, B. G. Chen, and V. Vitelli, Nat. Phys. **11**, 153 (2015).
- [37] Pai Wang, Ling Lu, and Katia Bertoldi, Phys. Rev. Lett. **115**, 104302 (2015).
- [38] D. Z. Rocklin, B. Gin-ge Chen, M. Falk, V. Vitelli, and T. C. Lubensky, Phys. Rev. Lett. **116**, 135503 (2016).
- [39] Olaf Stenull, C. L. Kane, and T. C. Lubensky, Phys. Rev. Lett. **117**, 068001 (2016).
- [40] A. V. Chumak, V. I. Vasyuchka, Serga, A. A. Hillebrands, Nature Phys. **11**, 453 (2015).
- [41] I. Dzyaloshinsky, J. Phys. Chem. Solids **4**, 241 (1958).
- [42] T. Moriya, Phys. Rev. **120**, 91 (1960).
- [43] A. Mook, J. Henk, and I. Mertig, Phys. Rev. Lett. **117**, 157204 (2016).
- [44] Ying Su, X. S. Wang, X. R. Wang, Phys. Rev. B **95**, 224403 (2017).
- [45] A. Mook, J. Henk, and I. Mertig, Phys. Rev. B **95**, 014418 (2017).
- [46] Fei-Ye Li, Yao-Dong Li, Yong Baek Kim, Leon Balents, Yue Yu, and Gang Chen, Nature Communications **7**, 12691 (2016).
- [47] M. Matsuda, M. Azuma, M. Tokunaga, Y. Shimakawa, and N. Kumada, Phys. Rev. Lett. **105**, 187201 (2010).
- [48] D. E. McNally, J. W. Simonson, J. J. Kistner-Morris, G. J. Smith, J. E. Hassinger, L. DeBeer-Schmitt, A. I. Kolesnikov, I. A. Zaliznyak, and M. C. Aronson, Phys. Rev. B **91**, 180407(R) (2015).
- [49] A. R. Wildes, B. Roessli, B. Lebech, and K. W. Godfrey, J. Phys.: Condens. Matter **10**, 6417 (1998).
- [50] A. Wiedenmann, J. Rossat-Mignod, A. Louisy, R. Brec, and J. Rouxel, Solid State Commun. **40**, 1067 (1981).
- [51] K. Okuda, K. Kurosawa, S. Saito, M. Honda, Z. Yu, and M. Date, J. Phys. Soc. Jpn. **55**, 4456 (1986).
- [52] A. R. Wildes, K. C. Rule, R. I. Bewley, M. Enderle, and T. J. Hicks, J. Phys.: Condens. Matter **24**, 416004 (2012).
- [53] A. C. Gossard, V. Jaccarino, and J. P. Remeika, Phys. Rev. Lett. **7**, 122 (1961).
- [54] H. L. Davis and Albert Narath, Phys. Rev. **134**, A433 (1964).
- [55] N. Rogado, Q. Huang, J. W. Lynn, A. P. Ramirez, D. Huse, and R. J. Cava, Phys. Rev. B **65**, 144443 (2002).
- [56] L.P. Regnault, J. Y. Henry, J. Rossat-Mignod, J. Magn.

- Magn. Mater. **15**, 1021 (1980).
- [57] D. Boldrin, B. Fak, M. Enderle, S. Bieri, J. Ollivier, S. Rols, P. Manuel, and A. S. Wills, Phys. Rev. B **91**, 220408(R) (2015).
 - [58] Daniel Grohol, Daniel G. Nocera, and Dimitris Papoutsakis, Phys. Rev. B **67**, 064401 (2003).
 - [59] Masahide Nishiyama, Satoru Maegawa, Toshiya Inami, and Yoshio Oka Phys. Rev. B **67**, 224435 (2003).
 - [60] M. G. Townsend, G. Longworth, and E. Roudaut, Phys. Rev. B **33**, 4919 (1986).
 - [61] S.-H. Lee, C. Broholm, M. F. Collins, L. Heller, A. P. Ramirez, Ch. Kloc, E. Bucher, R. W. Erwin, and N. Lacey, Phys. Rev. B **56**, 8091 (1997).
 - [62] T. Inami, T. Morimoto, M. Nishiyama, S. Maegawa, Y. Oka, and H. Okumura Phys. Rev. B **64**, 054421 (2001).
 - [63] K. Matan, D. Grohol, D. G. Nocera, T. Yildirim, A. B. Harris, S. H. Lee, S. E. Nagler, and Y. S. Lee, Phys. Rev. Lett. **96**, 247201 (2006).
 - [64] D. Grohol, K. Matan, J.H. Cho, S.-H. Lee, J.W. Lynn, D.G. Nocera, Y.S. Lee, Nature Materials **4**, 323 (2005).
 - [65] Y. -Z. Zheng, M. -L. Tong, W. Xue, W. -X. Zhang, X. -M. Chen, Fe. Grandjean, G. J. Long, Angew. Chem., Int. Ed. **46**, 6076 (2007).
 - [66] J. Fransson, A. M. Black-Schaffer, and A. V. Balatsky, Phys. Rev. B **94**, 075401 (2016).
 - [67] Yasumasa Hasegawa, Rikio Konno, Hiroki Nakano, Mahito Kohmoto, Phys. Rev. B **74**, 033413 (2006).
 - [68] B. Wunsch, F. Guinea, F. Sols, New J. Phys. **10**, 103027 (2008).
 - [69] F. Guinea, M. I. Katsnelson, and A. K. Geim, Nature Physics **6**, 30 (2009).
 - [70] Su-Yang Xu, Y. Xia, L. A. Wray, D. Qian, Shuang Jia, J. H. Dil, F. Meier, J. Osterwalder, B. Slomski, H. Lin, R. J. Cava, M. Z. Hasan, Science **332**, 560 (2011).
 - [71] Hua Chen, Qian Niu, and A. H. MacDonald, Phys. Rev. Lett. **112**, 017205 (2014).
 - [72] P. A. Maksimov and A. L. Chernyshev, Phys. Rev. B **93**, 014418 (2016).
 - [73] Susumu Okubo *et al*, Phys. Rev. B **86**, 140401(R) (2012).
 - [74] Patrick A. Lee, Science **321**, 1306 (2008).
 - [75] Lucile Savary and Leon Balents, Rep. Prog. Phys. **80**, 016502 (2017).
 - [76] Kai Sun, W. Vincent Liu, Andreas Hemmerich, S. Das Sarma, Nature Physics **8**, 67 (2012).
 - [77] M. Elhajal, B. Canals, and C. Lacroix, Phys. Rev. B **66**, 014422 (2002).
 - [78] O. Cépas, C. M. Fong, P. W. Leung, and C. Lhuillier Phys. Rev. B **78**, 140405(R) (2008).
 - [79] A. B. Harris, C. Kallin, and A. J. Berlinsky, Phys. Rev. B **45**, 2899 (1992).
 - [80] A. Scheie, M. Sanders, J. Krizan, Y. Qiu, R.J. Cava, C. Broholm, Phys. Rev. B **93**, 180407 (2016).
 - [81] S. A. Owerre, J. Phys.: Condens. Matter **29**, 03LT01 (2017).
 - [82] S. A. Owerre, Phys. Rev. B **95**, 014422 (2017).
 - [83] Yoko Miura, Riu Hirai, Yoshiaki Kobayashi, and Masatoshi Sato, J. Phys. Soc. Jpn. **75**, 084707 (2006).
 - [84] N. Goldman, E. Anisimovas, F. Gerbier, P. Ohberg, I. B. Spielman, G. Juzeliunas, New J. Phys. **15**, 013025 (2013).
 - [85] Shunsuke Furukawa and Masahito Ueda, New J. Phys. **17**, 115014 (2015).
 - [86] Congjun Wu, Phys. Rev. Lett. **95**, 266404 (2005).
 - [87] D. van Oosten, P. van der Straten, and H. T. C. Stoof, Phys. Rev. A **63**, 053601 (2001).
 - [88] D. B. M. Dickerscheid, D. van Oosten, P. J. H. Denteneer, and H. T. C. Stoof Phys. Rev. A **68**, 043623 (2003).
 - [89] D. Jaksch and P. Zoller, New J. Phys. **5**, 56 (2003).
 - [90] M. Aidelsburger, M. Atala, S. Nascimbéne, S. Trotzky, Y.-A. Chen, and I. Bloch, Phys. Rev. Lett. **107**, 255301 (2011).
 - [91] Markus Greiner, Olaf Mandel, Tilman Esslinger, Theodor W. Hänsch, and Immanuel Bloch, Nature **415**, 39 (2002).
 - [92] Eugene Demler and Fei Zhou, Phys. Rev. Lett. **88**, 163001 (2002).
 - [93] Immanuel Bloch, Nature Physics **1**, 23 (2005).
 - [94] Gregor Jotzu, Michael Messer, Rémi Desbuquois, Martin Lebrat, Thomas Uehlinger, Daniel Greif, and Tilman Esslinger, Nature **515**, 237 (2014).
 - [95] T. Matsubara and H. Matsuda, Prog. Theor. Phys. **16**, 569 (1956).
 - [96] Ivana Vasić, Alexandru Petrescu, Karyn Le Hur, and Walter Hofstetter, Phys. Rev. B **91**, 094502 (2015).
 - [97] Huaiming Guo, Yuekun Niu, Shu Chen, and Shiping Feng, Phys. Rev. B **93**, 121401(R) (2016).
 - [98] S. A. Owerre, J. Phys.: Condens. Matter **28**, 436003 (2016).
 - [99] Luuk J. P. Ament, Michel van Veenendaal, Thomas P. Devereaux, John P. Hill, and Jeroen van den Brink, Rev. Mod. Phys. **83**, 705 (2011).
 - [100] Khalil Zakeri, Physics Reports **545**, 47 (2014).